Lab on a Chip

PAPER

View Article Online
View Journal | View Issue

Cite this: *Lab Chip*, 2014, **14**, 4426

Rapid determination of cell mass and density using digitally controlled electric field in a microfluidic chip

Yuliang Zhao,[a] Hok Sum Sam Lai,[a] Guanglie Zhang,*[a] Gwo-Bin Lee[b] and Wen Jung Li*[a]

The density of a single cell is a fundamental property of cells. Cells in the same cycle phase have similar volume, but the differences in their mass and density could elucidate each cell's physiological state. Here we report a novel technique to rapidly measure the density and mass of a single cell using an optically induced electrokinetics (OEK) microfluidic platform. Presently, single cellular mass and density measurement devices require a complicated fabrication process and their output is not scalable, *i.e.*, it is extremely difficult to measure the mass and density of a large quantity of cells rapidly. The technique reported here operates on a principle combining sedimentation theory, computer vision, and microparticle manipulation techniques in an OEK microfluidic platform. We will show in this paper that this technique enables the measurement of single-cell volume, density, and mass rapidly and accurately in a repeatable manner. The technique is also scalable – it allows simultaneous measurement of volume, density, and mass of multiple cells. Essentially, a simple time-controlled projected light pattern is used to illuminate the selected area on the OEK microfluidic chip that contains cells to lift the cells to a particular height above the chip's surface. Then, the cells are allowed to "free fall" to the chip's surface, with competing buoyancy, gravitational, and fluidic drag forces acting on the cells. By using a computer vision algorithm to accurately track the motion of the cells and then relate the cells' motion trajectory to sedimentation theory, the volume, mass, and density of each cell can be rapidly determined. A theoretical model of micro-sized spheres settling towards an infinite plane in a microfluidic environment is first derived and validated experimentally using standard micropolystyrene beads to demonstrate the viability and accuracy of this new technique. Next, we show that the yeast cell volume, mass, and density could be rapidly determined using this technology, with results comparable to those using the existing method *suspended microchannel resonator*.

Received 9th July 2014,
Accepted 4th September 2014

DOI: 10.1039/c4lc00795f

www.rsc.org/loc

Introduction

The mass of a single cell is the most basic physical property indicating the cellular metabolic rate and its fate,[1] while the density of a single cell reveals more detailed information on the cell's state.[2,3] In relation to cell physiology, the mass and density of a single cell also reveal the nature of cell cycle regulation[4–6] more closely than indirect parameters such as cellular shape or non-aqueous mass. The measurement of cell mass and density can also provide a direct and effective evaluation mechanism to monitor cell responses to external stimuli such as drugs and environmental changes.[3]

Recently, as a tool of proteomics, mass spectrometry utilizing transition element isotopes has been used for cellular mass measurement.[7–9] In addition, interferometric microscopy based on the relationship between the quantitative phase image of a cell and its non-aqueous content is used to measure the "dry mass" of a cell.[2,10] Although these two methods can measure cellular mass in an indirect way, both are restricted by their complicated mapping processes and lack of density information.

Another technique to determine cell mass is using a suspended microchannel resonator (SMR),[11] which is a cantilever resonator[12,13] integrated into a microchannel and can be used as a density sensor. A research group led by S. R. Manalis has done tremendous research work in the past decade using this method to measure the density of a single cell.[14–16] The cell mass is obtained by calculating the cell volume using the resistive pulse (Coulter) technique or by passing the cell through two different types of mediums in

[a] *Dept. of Mechanical and Biomedical Engineering, City University of Hong Kong, Hong Kong. E-mail: gl.zhang@cityu.edu.hk, wenjli@cityu.edu.hk*
[b] *Dept. of Power Mechanical Engineering, National Tsing Hua University, Hsinchu 30013, Taiwan*

the SMR.[17] Because of the complicated fabrication process involved and the requirement that cells must be captured and passed through the resonators, this technology is less practical when the mass of many cells needs to be determined simultaneously. More recently, a pedestal resonant sensor (PRS)[18–20] has been developed by another excellent research group led by R. Bashir with a similar measuring principle. Although it has a lower resolution (10^{-10} g) in the case of mass measurement, it is more suitable for measuring adherent cells and effective in measuring the stiffness of a cell.[5,19]

On the other hand, the classical and established method of measuring the population density of cells is using density gradient centrifugation.[21–23] During sedimentation, the cells settle to an equilibrium position in a density gradient where they are equivalent to their own natural buoyant density. Combined with their volume, the average mass of the cells can be calculated. However, due to its low accuracy, *i.e.*, the density and mass obtained are averaged values of a group of cells, this technique has not much success in measuring the density and mass of a single cell. Even now, researchers have continued to measure cellular sedimentation velocity[24,25] of cells rather than single cell density and mass. One reason is that it is difficult for a single cell to settle in the same way repeatedly. Furthermore, taking into account the large variations in the mass and density of cells, the average value of mass from many cells may not provide enough information regarding the true physiological state of a cell. Therefore, the direct, rapid and repeatable measurement for buoyancy mass and density of a single cell is still a technical challenge.

In this paper, we present the possibility of using optically induced electrokinetics (OEK) as a practical solution to this classical problem. OEK is essentially a dielectrophoresis (DEP) system but it uses digitally controlled and optical images to define virtual electrodes instead of metal electrodes. The basic principle was first reported by P. Y. Chiou[26] *et al.* (2005) and has sometimes been referred to as "optoelectronic tweezers". Based on OEK technology, single and parallel manipulation of cells[27] have been reported, including cell transport,[28,29] separation,[30,31] rotation[32] and patterning.[33]

The operation principle and the structure of the OEK chip make it extremely difficult to use a lateral microscope for observing the sedimentation of the cells laterally. In our work, a monocular microscope system placed on top of the OEK chip was adapted to observe cellular sedimentation displacement in the vertical direction. Other researchers have tracked micron-scale and nano-scale particles under a single camera microscope using fluorescence[34] and multiplane[35] methods. We have shown that just by using an image-matching algorithm, we could track the vertical trajectory of micron-scale particles accurately. The defocused images of microparticles at different heights captured by a microscope appeared differently because of the changed diffractive and refractive light paths. Hence, a microparticle's vertical position could be obtained by comparing the particle's time-sequence images captured during its motion trajectory with the static calibrated images captured at known heights, without any change in hardware configuration.

In this paper, we will show that the mass and density of a single cell could be measured by utilizing an OEK system and the simple micro-vision technique discussed above. First, the density and mass of micropolystyrene beads were measured to validate the method. Two types of microbeads (radii of 5.26 μm and 10.42 μm) were first tested before experiments on cells were conducted. A high-speed (maximum 48 fps) and high-resolution (1280 × 1024 pixels) camera was used to record the images of the beads at different heights in an OEK chip in a time sequence. To calibrate the height of microbeads from a reference plan, static bead images at different heights from a reference plan were obtained by keeping the bead on the OEK chip's surface, while the objective stage of the microscope was moved vertically. Since the movement of the stage is controlled to an accuracy of 0.1 μm in the vertical direction, the standard images captured by the camera could provide the same vertical displacement resolution if the images are processed appropriately. Hence by comparing the static (calibration) images with the images captured from actual experiments, the height of a microparticle as a function of time could be obtained by analyzing the sequence of images captured from a dynamically moving microparticle. Hence, the bead's displacement trajectory, velocity, and acceleration during the sedimentation process inside the OEK chip could be deduced. According to sedimentation theory, the viscous force varies with the distance when micron-sized spherical objects are falling perpendicular to a single, infinite plane. To describe the changing viscosity force, which dominates the sedimentation process, a correction factor for Stokes' law is required and was also experimentally determined in our work. We will show in the Results and discussion section that the accurate determination of this correction factor will allow the matching of experimental results with classical analytical results for the sedimentary trajectories of the beads and cells in an OEK chip. To demonstrate that this OEK-based cell mass and density measurement technique can be generalized to measure non-spherical cells, we tested yeast cells following the same experimental procedure for the beads. The measurement results of the specific cellular mass and density of 44 individual yeast cells are given in the Results and discussion section. We will show that the density and mass of yeast cells obtained using the OEK-based methods reported here are close to the values reported by others, as compared in the table below (Table 1).

Method

The OEK system

Fig. 1 illustrates the OEK system and the geometrical configuration of the OEK chip, which were described in more detail in our prior work related to cancer cell patterning[33] and

Table 1 Comparison of yeast cell mass/density measured by the OEK-based method proposed in this paper with the SMR method

Method	Reference	Density (g ml^{-1})	Volume (μm^3)	Buoyant mass (pg)
SMR	Bryan *et al.* (2010) ref. 14	1.08–1.13	40–260	4–17
OEK	This paper	1.04–1.13	85–350	6–36

controlling fluidic interface instability.[36] The microfluidic chamber is constructed from two pieces of indium tin oxide (ITO)-coated glass (3 cm × 3 cm × 1 mm). The height of the medium (DI water) between them is about 60 μm with a relative permittivity of 80 and a conductivity of 1.3×10^{-2} S m^{-1}. A 1 μm thick layer of hydrogenated amorphous silicon (a-Si:H) is deposited at the bottom ITO glass substrate. When an AC voltage bias is applied between these two ITO layers, no electrical conduction path is formed until a digital image is projected onto the surface of the a-Si:H layer. Since the light image locally increases the electrical conductivity of a-Si:H, virtual electrodes are formed in the illuminated area. In Fig. 1, the light spot (in green) controlled by the computer is generated by the projector. After being shrunk by the optical condenser, it passes through the ITO glass and is patterned onto the a-Si:H layer. Compared to the dark area, the green area forms a virtual electrode which polarizes the objects around it, similar to a metal electrode. The polarized micro-objects are attracted or repelled by the DEP force generated by the induced non-uniform electric field. While the microparticle on top of the green area is lifted into the fluidic medium, the microparticle that is far from the green electrode will remain on the surface of the OEK chip. Compared to the complicated fabrication of traditional DEP and microfluidic techniques, selective manipulation of the micro-objects becomes simple and flexible using the OEK system.

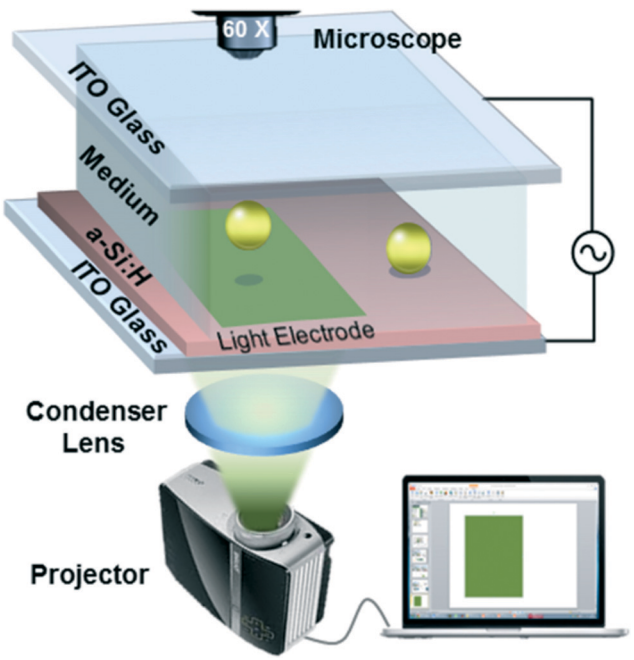

Fig. 1 Illustration of the OEK system and the OEK chip. The experimental system consists of a computer, a signal generator, a display projector, and a microscope; the enlarged illustration of the OEK chip details the different layer structures.

Manipulation of cells and beads under the OEK system

When light is projected on a particular area on the photoconductive layer, a localized DEP field is generated across the lighted area of the conductive layer. Assuming that a microparticle suspended in the medium is perfectly spherical, the time-averaged DEP force acting on the particle in an OEK device can be expressed as[37]

$$F_{DEP} = 2\pi\varepsilon_m r^3 \mathrm{Re}[K(\omega)]\nabla|E| \quad (1)$$

where ε_m is the dielectric permittivity of the medium, r is the radius of the particle, $K(\omega)$ is the Clausius–Mossotti (CM) factor, ω is the applied angular frequency across the medium, and E is the electric field. The CM factor can then be expressed as

$$K(\omega) = \frac{\varepsilon_p^* - \varepsilon_m^*}{\varepsilon_p^* + 2\varepsilon_m^*} \quad (2)$$

where $\varepsilon_i^* = \varepsilon_i - j\sigma_i/\omega$, i = p or m, denoting the particles and the medium, respectively, and σ is the conductivity. However, a cell commonly consists of a nucleus, cytoplasm, and other organelles and is surrounded by a membrane. It can be considered as a single-shell model instead of a homogeneous sphere. An approximation of the effective complex permittivity of spherical-like cells[38] is given by

$$\varepsilon_p^* = c_s r\left[\frac{j\omega\tau_c + 1}{j\omega(\tau_s + \tau_c) + 1}\right] \quad (3)$$

where c_s is the surface capacitance of the membrane, and $\tau_s = c_s r/\sigma_p$ and $\tau_c = \varepsilon_p/\sigma_p$. Based on the particle's dielectric properties, the degree of forces affecting them can be adjusted by controlling the frequency of the AC voltage applied across the OEK chip. Fig. 2 illustrates the manipulation of the microparticles under the OEK system and the main forces acting on them in the OEK platform. If the particle is above the center of the electrode and the electrode is large enough, then the edge area of the electrode where the DEP force is not vertical can be ignored. The polarized microparticles will experience mainly a vertical lift DEP force. By adjusting the frequency and voltage magnitude of the electric field applied to the OEK chip, the projected electrode can produce a large enough DEP force to overcome the viscosity drag force and the

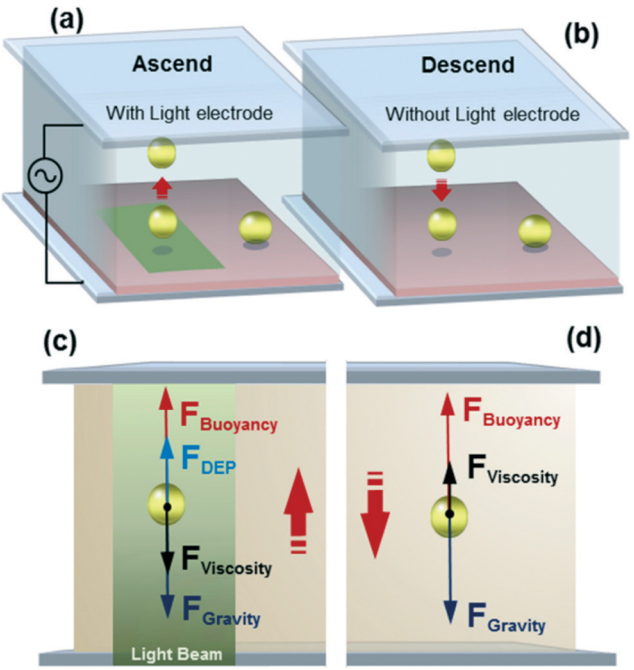

Fig. 2 Illustration of the manipulation of microparticles. (a) When a light beam is projected onto the OEK chip, the particle is lifted up and (b) when there is no light projected, the particle starts to sediment. The forces acting on the particle, when it is (c) rising and (d) falling.

sedimentation force (*i.e.*, gravity and buoyancy forces) to lift the microparticles to a suitable height.

Measurement principle of buoyancy mass and density

The principle of manipulating microparticles in an OEK environment has been discussed in the past already by many other researchers.[39–41] Besides the forces mentioned above, forces due to thermal effects, electro-osmosis, Brownian motion, and particle-to-particle interactions can all be neglected under our experimental conditions.[23] These forces have much lower orders of magnitude ($<10^{-16}$ N) than the viscosity force, buoyancy force and gravitational force which have orders of magnitude of about 10^{-12} N. The sedimentary force is the resultant effect of the buoyancy and gravitational forces which can be described as

$$F_{\text{Sedimentary}} = F_{\text{Gravity}} - F_{\text{Buoyancy}} = \frac{4}{3}\pi r^3 \left(\rho_{\text{Particle}} - \rho_{\text{Medium}}\right) g \quad (4)$$

where ρ_{Particle} is the density of the particle, ρ_{Medium} is the density of the solution and $\rho_{\text{Particle}} - \rho_{\text{Medium}}$ is commonly defined as the buoyancy density. The buoyancy mass is the buoyancy density multiplied by the volume. r is the radius of the particle. During sedimentation, the initial vertical state equation of a microparticle (of mass m) can be expressed as

$$m\frac{\mathrm{d}u}{\mathrm{d}t} = F_{\text{Sedimentary}} + F_{\text{Viscosity}} \quad (5)$$

where u is the vertical velocity of the particle and $F_{\text{Viscosity}}$ is the viscosity force exerted by the medium. According to Stokes' law,[42] the equation below can be used to describe the viscosity force acting on a sphere as it moves with velocity u in a medium,

$$F_{\text{Viscosity}} = 6\pi r\eta u K \quad (6)$$

where η is the dynamic viscosity of the fluid medium (at 20 °C, the viscosity of water[43] (1.002) is used in our calculations) and K is the correction factor of Stokes' law when a sphere is falling perpendicular to an infinitely long plane surface. Then eqn (5) can be expressed as

$$m\frac{\mathrm{d}u}{\mathrm{d}t} = \frac{4}{3}\pi r^3 \left(\rho_{\text{Cell}} - \rho_{\text{Medium}}\right) g + 6\pi r\eta u K \quad (7)$$

The function of the velocity can be solved from eqn (7) as

$$u(t) = \frac{2r^2 g\left(\rho_{\text{Cell}} - \rho_{\text{Medium}}\right)}{9\eta K}\left(1 - e^{-\frac{t}{\tau}}\right) \quad (8)$$

where $\tau = m/6\pi R\eta K$. Since $\tau \approx 10^{-6}$ seconds, this means that the acceleration time, t, is too fast to be observed and the inertia force can be neglected. Thus the classical equation for the particle velocity can be simplified as

$$u(t) = \frac{2r^2 g\left(\rho_{\text{Cell}} - \rho_{\text{Medium}}\right)}{9\eta K} \quad (9)$$

Then the density of cells can be expressed as

$$\rho_{\text{Cell}} = \frac{9\eta K u}{2r^2 g} + \rho_{\text{Medium}} \quad (10)$$

Hence, if the falling velocity u and the correction factor K of Stokes' law can be obtained, the density of the cell can be calculated using the above equation. Consequently, if the volume of the cell is known, the cell's buoyancy mass can be calculated. However, as the spherical particle is falling perpendicularly towards an infinitely long solid plane, the value of the correction factor K of Stokes' law will increase, while the sedimentary velocity will decrease. According to Taylor's classical lubrication theory,[44] the correction factor K in Stokes' law is equal to r/h, where h is defined as the gap between the bottom of the falling sphere and the solid plane; that is, as the spherical particle approaches the surface of the plane, $r/h \to \infty$. Our experimental data shows that if the falling distance of the particle is close to the radius of the particle (about 5–10 μm) and if there is no wall around the settling sphere, the correction factor K can be expressed as

$$K = a\frac{r}{h} \quad (11)$$

where a is a constant dictated by the size and density of the sphere. Substituting eqn (11) into eqn (9), then the falling height of the sphere can be modelled as an exponential function of time. After fitting the experimental data of the density of known spheres to the height–time function, the constant a can be deduced from the time constant of the exponential function.

Trajectory in the vertical direction

Studies on Depth-from-Defocus (DFD)[45] have been applied in the past in particle tracking with nanometer resolution.[46] In order to minimize the calibration process required for the configuration of the microscope system, an image-matching method is used to obtain the height of the particles suspended in the fluidic medium of the OEK chip. The main idea is to compare the images of the settling particles with the standard (static) images of particles of known heights. This method requires more computational complexity, but it enables accurate displacement resolution.

As shown in Fig. 3, the standard images of a bead at different heights are shown on the left side, while the images from a dynamically moving bead are compared to the standard images to determine its trajectory as a function of time. The microscope (NIKON Ti-E) used in our experiments has a stage with 25 nm resolution in the vertical direction. First, the standard (static/calibration) images of a spherical particle are captured at different heights with incremental heights of 0.1 μm. The zero point image (the bottom image in Fig. 3) was selected at the height where the particles have the most clear image, *i.e.*, in focus. Then, the manipulation stage of the microscope was moved away from the objective lens at step increments of 0.1 μm. At each incremental step, an image of the particle of interest was obtained. The incremental steps of the manipulation stage were executed by the microscope system automatically. The range of the incremental images obtained spans from 2 μm below the reference point (zero point image) to 10 μm above the reference point. Therefore, there are 121 standard images that can be used to compare to time-lapsed images of falling particles to obtain the height of particles in each image frame.

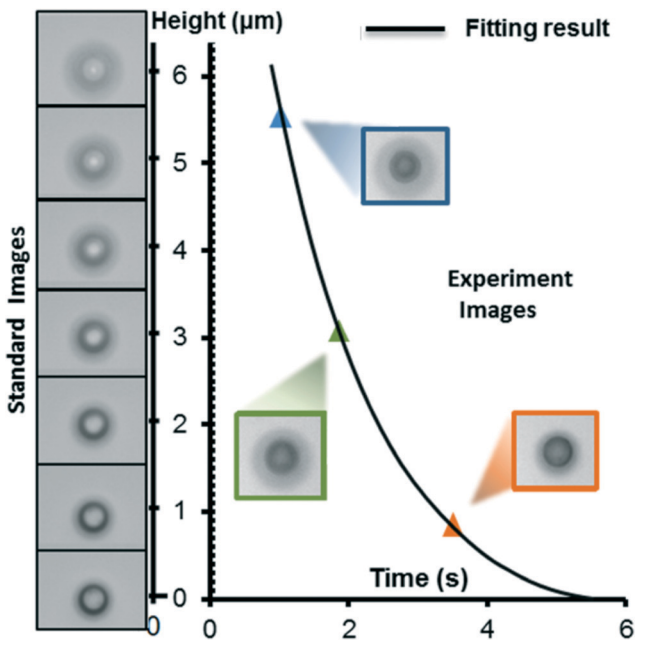

Fig. 3 Illustration of particle height determination by matching the dynamic images with standard images of known heights.

Cell culture

Yeast cells (#20867 obtained from ATCC, USA) were cultured in a shaking incubator (Model KS 4000i, IKA). Yeast Extract Peptone Dextrose Medium (YEPD) with 200 mcg ml^{-1} Geneticin was used as the culture medium. First, 5–6 ml of culture medium was added to a 25 cm^2 flask. Then, 200 μl of the prepared suspension solution containing yeast cells was added to the flask. All of these steps were performed in a biological safety cabinet (Model Heracell® 150i, Thermo Scientific). The flask and its contents were kept at the recommended temperature (28–30 °C) in an incubator with a shaking speed of 220 rpm. The medium was refreshed every two days.

Results and discussion

Measurement of standard particles

As mentioned earlier, before measuring the density and mass of the cell, standard microbeads with a known density and size are used to calibrate the correction factor of Stokes' law. Although the function of this correction factor has already been calculated and expressed by many researchers in the past, the actual environment of our experiments is different from those of reported studies. First, comparing the radii of the particles to the falling distances, researchers have reported either $h \gg r$ (ref. 47) or $r \gg h$,[48,49] while in our experiments the falling distance was kept close to the beads' radius. Second, the radius of the sphere in our experiment was about 5–10 μm, which has not been analyzed in the past. In the low Reynolds number range, most of the experiments in the past mainly focused on the spheres with a millimeter-scale diameter.[48–50]

After comparing the time-sequence images of a falling bead with standard images at different heights, the displacement of the bead between any consecutive two image frames can be easily obtained. Combining the elapsed time information recorded in the video (sequence of images), a distance–time plot (s–t plot) is obtained from the cell sedimentation motion. The s–t plots are shown in Fig. 4.

The entire process of experimentation can be divided into four stages, representing four different motion states of the beads. In the first stage, no light was projected onto the OEK chip, thus there was no DEP force acting on the beads, and hence no displacement change. In stage II, when light was projected, the microbeads were lifted by the DEP force. Different beads were lifted up by different strengths of DEP force, depending on their initial position on the projected image. This ascending phase approximately takes 1–3 s depending on each cell's trajectory. In stage III, the descending phase, the projected light was shut off, *i.e.*, no voltage was applied to the OEK chip, and all of the beads fell towards the bottom of the OEK chip. During this sedimentation period, the density and mass of the beads are the crucial factors governing the falling velocity. According to eqn (10), if the density and the radius of beads are the same, they will fall at the same rate. The experimental data shown in Fig. 4 reflect the free fall motion of the beads which lasts for 6 s to

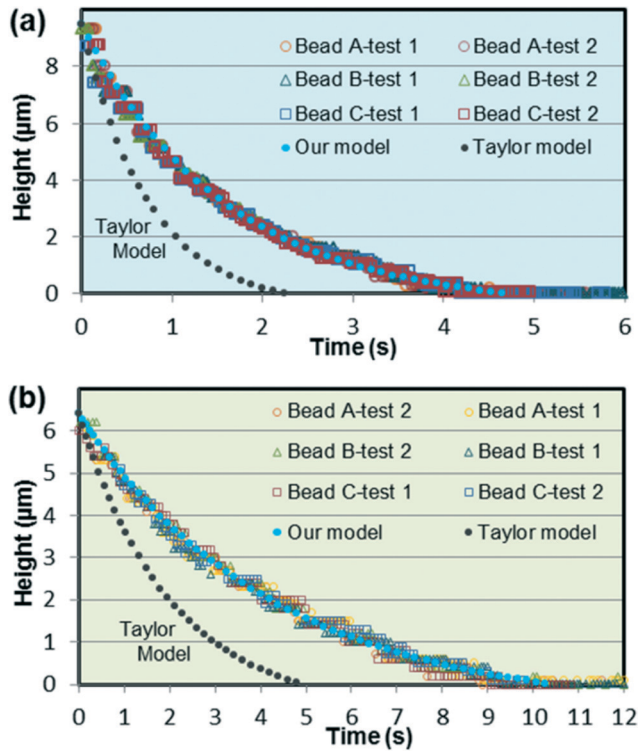

Fig. 4 Time-lapsed height variation plots of two different types of microbeads with radii of (a) 10.42 μm and (b) 5.26 μm. Each figure shows experimental data for 3 different polystyrene spheres of the same size, with 2 experiments performed on each sphere. The blue solid dotted lines are the results of curve fitting to eqn (11), with both of them calculated using the same constant a = 2.0. The black dotted lines are the curves calculated from Taylor's classical lubrication theory, marked as the Taylor Model.

12 s during this stage. Finally, after the beads landed on the plane, there was no further displacement; the beads settled down on the bottom of the OEK chip. Therefore, a single cycle for cell motion image capturing takes about 15 s. In addition, the computational time to process the images for one single cycle takes about 3.5 s. Hence, the approximate time to determine the mass/density of a single cell will take ~18.5 s using the proposed method. As discussed above, the proposed method can be used to measure the density/mass of multiple cells simultaneously – the quantity of cells measured simultaneously depends on the field-of-view of the microscope and camera used. Our experiment was performed under a 60× lens, which has a field-of-view that contained at least 100 yeast cells. If a lower magnification lens and a broader field-of-view camera are used, the quantity of cells whose density and mass could be measured simultaneously could be increased significantly.

So far, to the best of our knowledge, there is no experimental data on obtaining the correction factor K for Stokes' law for micron-scale spheres. Our method presented above provides a reliable way of measuring the correction factor K for Stokes' law. Considering that the diameter of the test yeast cell is about 5.5–8.8 μm, the correction factor a = 2.0 was chosen based on the testing results of similar beads.

Mass and density of yeast cells

The sedimentation experiments performed on yeast cells were similar to those performed on microbeads, except that the shapes of most of the yeast cells were ellipsoidal rather than perfect spheres. Therefore, an additional process is required to make each yeast cell stand "upright" before the cell is lifted up in the fluidic medium. Fig. 5 shows this additional process required for yeast cell experiments.

The "upright" posture of yeast cells on the chip's bottom surface is required while capturing their static images with different heights. This could be done by adjusting the magnitude of the AC voltage applied across the chip, *i.e.*, a voltage significant enough to align the cell's orientation to the electric field lines but not enough to apply enough DEP force to lift the cell. To calculate the volume of the yeast cells, the axes of the ellipsoidal cells were measured in different postures. In Fig. 5(a), A1, B1, C1 are three yeast cells in their initial states while being projected by the "optical electrode"; D1 cell is at a distance away from the electrode. But at this stage no voltage across the OEK chip was applied, thus there was no OEK force affecting the A1, B1, and C1 cells. Fig. 5(b) is the image when there is voltage applied across the OEK chip. The three cells on the "optical electrode" are lifted up by the optically induced DEP force. A2, B2, and C2 show the corresponding images of the upright state of the original A1, B1, and C1 yeast cells, respectively. Since the DEP force in the dark area far from the "optical electrode" is small, the

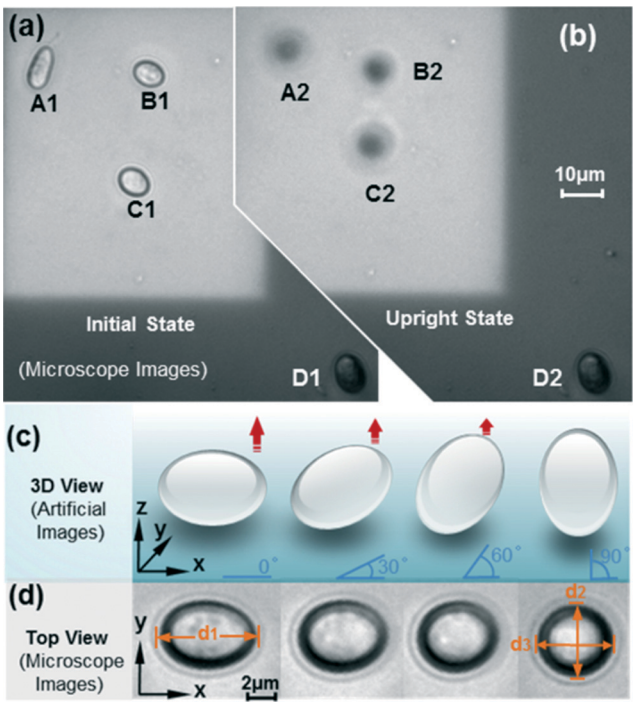

Fig. 5 Microscope images of selective and multiplicative manipulation of yeast cells being lifted up from (a) the initial state to (b) the upright state (*i.e.*, 90° tilt angle). (c) Illustration of the egg-like states of a yeast cell with tilt angles of 0°, 30°, 60° and 90°. (d) Microscope images of the top views of a yeast cell with a tilt angle of 0°, 30°, 60° and 90°.

orientation of yeast cell D1 is unaffected and hence the image of D2 is similar to that of D1.

Once the yeast cell was lifted into the fluidic medium to a particular height, the projection light image was turned off, and the yeast cell was allowed to "free fall" in the medium. Since no DEP force acts on the cell any more, gravity force will overcome the buoyant and viscosity forces and dominate the falling process. Fig. 6 shows the details of a yeast cell's falling sequence in the medium inside an OEK chip.

For an ellipsoid[51] moving lengthwise in the medium, the translational friction factor f can be described as $f = 4\pi\eta a_1/(\ln(2a_1/a_2) - 0.5)$ where a_1 is the longest semi-axis and a_2 is the shortest semi-axis. This expression is only valid when $a_1^2 \gg a_2^2$, while, in reality, the shortest axis of most of the yeast cells are, at the maximum, 25% shorter than the longest axis. The shapes of the yeast cells are closer to being spherical, thus an adjusted radius is used, *i.e.*, $r = \sqrt[3]{a_1 a_2 a_3}$.

Using the method described above, measurements for density and mass of 44 single yeast cells were performed (results shown in Fig. 7). The densities of yeast cells varied between 1.04 and 1.13 g cm^{-3}, while the buoyancy mass were in the range of 6–36 pg. This result broadly conforms to those of J. Lee[11] and A. K. Bryan.[14] Considering the differences in cell culturing methods, experimental medium types, cell cycle synchronicity and other conditions, these results demonstrate that our method is practical for measuring the density and mass of a single cell.

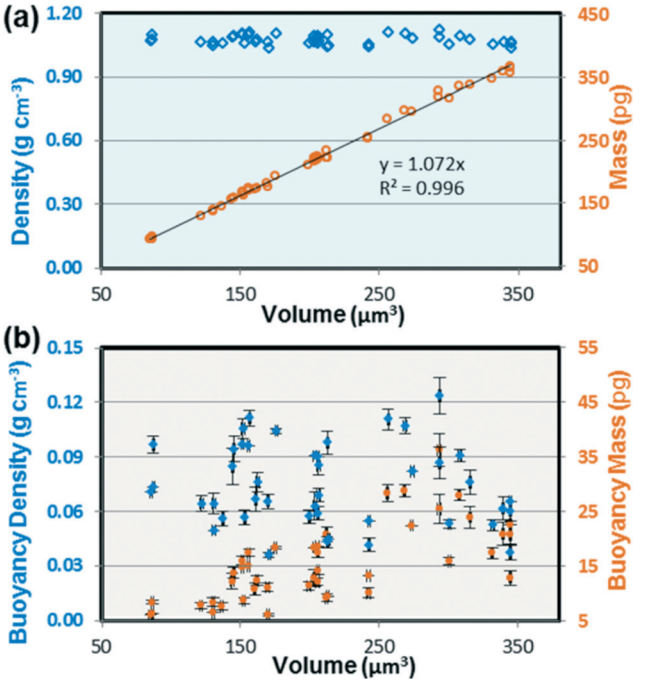

Fig. 7 Measured results of (a) densities, mass and volume and (b) buoyancy density (difference between cell density and medium density) and buoyancy mass (buoyancy density multiplied by cell volume) of 44 individual yeast cells.

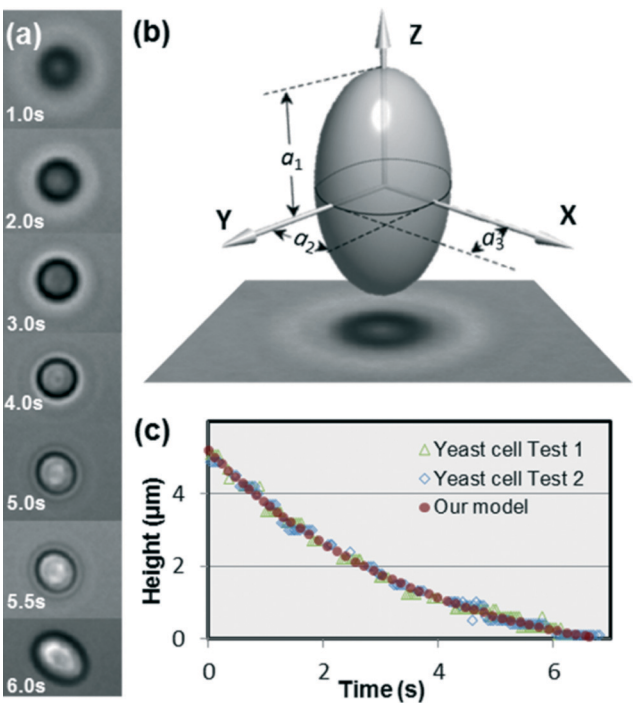

Fig. 6 (a) Microscope image sequence of a yeast cell falling in the medium. (b) Illustration of the relationship between the orientation of the yeast cell and its microscope image while falling. The radii a_1, a_2 and a_3 are the half of the values of diameters d_1, d_2 and d_3 measured in Fig. 5(d). (c) Repeated test results of one cell's time-lapsed height variation.

All of the data points in Fig. 7(b) are averaged values from 2–5 trials of experiments (where the motion of multiple yeast cells were tracked) under the same conditions. The average deviation is 5.2%. The key error source could come from the displacement measurement error caused by the determination of motion trajectory of each cell using a computational algorithm in analyzing the captured time-sequenced images. The brightness difference between images and random noises produced by the projector, CCD and other components of the image acquisition system could all contribute to the measurement error. In addition, in the non-uniform electrical field, cellular shape and size could change after prolonged polarization which could induce error in determining the cells' settling velocities.

Conclusions

A rapid single cell density and mass determination method has been developed by combining computer vision, microparticle manipulation, and sedimentation theory in an OEK microfluidic platform. This method is characterized for measuring microparticle's buoyancy mass and buoyancy density based on the classical buoyancy density sedimentation principle. The microparticles and cells could be lifted up by a digitally controlled DEP force in the medium of the OEK chip and then allowed to "free fall" to the OEK chip's surface. Utilizing an image processing technique, the falling motion

of the cells/microbeads could be tracked from sequential image frames. Based on the sedimentation theory of microparticles in solution, we successfully implemented a sedimentation velocity detection scheme to measure the buoyant density and mass of microparticles and yeast cells. We envision that this new method could potentially be widely used for determining the density and mass of many types of cells rapidly.

Acknowledgements

The authors gratefully acknowledge support from Hong Kong Research Grants Council (project no: CityU 118513 and 125513), Chinese Academy of Sciences – Croucher Funding Scheme for Joint Laboratories (project no: 9500011) and Nanshan Core Technology Breakthrough Project KC2013JSJS0003A. The authors would like to thank Dr. Fei Fei, Dr. Zhikun Zhan, and Mr. Yi Li, all from the City University of Hong Kong, for their insightful discussion on this research project.

Notes and references

1 M. Godin, F. F. Delgado, S. Son, W. H. Grover, A. K. Bryan, A. Tzur, P. Jorgensen, K. Payer, A. D. Grossman, M. W. Kirschner and S. R. Manalis, *Nat. Methods*, 2010, **7**, 387–390.
2 M. Mir, Z. Wang, Z. Shen, M. Bednarz, R. Bashir, I. Golding, S. G. Prasanth and G. Popescu, *Proc. Natl. Acad. Sci. U. S. A.*, 2011, **108**, 13124–13129.
3 W. H. Grover, A. K. Bryan, M. Diez-Silva, S. Suresh, J. M. Higgins and S. R. Manalis, *Proc. Natl. Acad. Sci. U. S. A.*, 2011, **108**, 10992–10996.
4 W. W. Baldwin and H. E. Kubitschek, *J. Bacteriol.*, 1984, **158**, 701–704.
5 K. Park, L. J. Millet, N. Kim, H. Li, X. Jin, G. Popescu, N. R. Aluru, K. J. Hsia and R. Bashir, *Proc. Natl. Acad. Sci. U. S. A.*, 2010, **107**, 20691–20696.
6 S. Son, A. Tzur, Y. Weng, P. Jorgensen, J. Kim, M. W. Kirschner and S. R. Manalis, *Nat. Methods*, 2012, **9**, 910–912.
7 R. Aebersold and M. Mann, *Nature*, 2003, **422**, 198–207.
8 S. C. Bendall, E. F. Simonds, P. Qiu, E. D. Amir, P. O. Krutzik, R. Finck, R. V. Bruggner, R. Melamed, A. Trejo, O. I. Ornatsky, R. S. Balderas, S. K. Plevritis, K. Sachs, D. Pe'er, S. D. Tanner and G. P. Nolan, *Science*, 2011, **332**, 687–696.
9 G. K. Behbehani, S. C. Bendall, M. R. Clutter, W. J. Fantl and G. P. Nolan, *Cytometry, Part A*, 2012, **81**, 552–566.
10 G. Popescu, Y. Park, N. Lue, C. Best-Popescu, L. Deflores, R. R. Dasari, M. S. Feld and K. Badizadegan, *Am. J. Physiol.*, 2008, **295**, C538–C544.
11 J. Lee, R. Chunara, W. Shen, K. Payer, K. Babcock, T. P. Burg and S. R. Manalis, *Lab Chip*, 2011, **11**, 645–651.
12 T.-I. Yin, Y. Zhao, J. Horak, H. Bakirci, H.-H. Liao, H.-H. Tsai, Y.-Z. Juang and G. Urban, *Lab Chip*, 2013, **13**, 834–842.
13 M. Khan, S. Schmid and P. Larsen, *Sens. Actuators, B*, 2013, **185**, 456–461.
14 A. K. Bryan, A. Goranov, A. Amon and S. R. Manalis, *Proc. Natl. Acad. Sci. U. S. A.*, 2010, **107**, 999–1004.
15 T. P. Burg, M. Godin, S. M. Knudsen, W. Shen, G. Carlson, J. S. Foster, K. Babcock and S. R. Manalis, *Nature*, 2007, **446**, 1066–1069.
16 M. Godin, A. K. Bryan, T. P. Burg, K. Babcock and S. R. Manalis, *Appl. Phys. Lett.*, 2007, **91**, 123121.
17 A. K. Bryan, V. C. Hecht, W. Shen, K. Payer, W. H. Grover and S. R. Manalis, *Lab Chip*, 2014, **14**, 569–576.
18 E. A. Corbin, L. J. Millet, K. R. Keller, W. P. King and R. Bashir, *Anal. Chem.*, 2014, **86**, 4864–4872.
19 G. Popescu, K. Park, M. Mir and R. Bashir, *Lab Chip*, 2014, **14**, 646–652.
20 S. Rashid, E. A. Corbin, B. R. Dorvel, L. J. Millet, P. King, W. P. King and R. Bashir, *Lab Chip*, 2014, **14**, 1401–1404.
21 M. Meselson, F. Stahl and J. Vinograd, *Proc. Natl. Acad. Sci. U. S. A.*, 1957, **43**, 581–588.
22 L. Hartwell, *J. Bacteriol.*, 1970, **104**, 1280–1285.
23 D. Maric, I. Maric and J. L. Barker, *Methods*, 1998, **16**, 247–259.
24 Z. Wang and J. M. Belovich, *Biotechnol. Prog.*, 2010, **26**, 1361–1366.
25 L. T. Bach, U. Riebesell, S. Sett, S. Febiri, P. Rzepka and K. G. Schulz, *Mar. Biol.*, 2012, **159**, 1853–1864.
26 P. Y. Chiou, A. T. Ohta and M. C. Wu, *Nature*, 2005, **436**, 370–372.
27 S.-B. Huang, M.-H. Wu, Y.-H. Lin, C.-H. Hsieh, C.-L. Yang, H.-C. Lin, C.-P. Tseng and G.-B. Lee, *Lab Chip*, 2013, **13**, 1371–1383.
28 K.-W. Huang, T.-W. Su, A. Ozcan and P.-Y. Chiou, *Lab Chip*, 2013, **13**, 2278–2284.
29 K.-W. Huang, Y.-C. Wu, J.-A. Lee and P.-Y. Chiou, *Lab Chip*, 2013, **13**, 3721–3727.
30 W. Liang, Y. Zhao, L. Liu, Y. Wang, Z. Dong, W. J. Li, G.-B. Lee, X. Xiao and W. Zhang, *PLoS One*, 2014, **9**, e90827.
31 Y. Zhao, W. Liang, G. Zhang, J. D. Mai, L. Liu, G.-B. Lee and W. J. Li, *Appl. Phys. Lett.*, 2013, **103**, 183702.
32 L.-H. Chau, W. Liang, F. W. K. Cheung, W. K. Liu, W. J. Li, S.-C. Chen and G.-B. Lee, *PLoS One*, 2013, **8**, e51577.
33 N. Liu, W. Liang, L. Liu, Y. Wang, J. Mai, G. Lee and W. Li, *Lab Chip*, 2014, **14**, 1367–1376.
34 M. Wu, J. W. Roberts and M. Buckley, *Exp. Fluids*, 2005, **38**, 461–465.
35 P. A. Dalgarno, H. I. C. Dalgarno, A. Putoud, R. Lambert, L. Paterson, D. C. Logan, D. P. Towers, R. J. Warburton and A. H. Greenaway, *Opt. Express*, 2010, **18**, 877–884.
36 F. Wang, H. Yu, N. Liu, J. D. Mai, L. Liu, G.-B. Lee and W. Jung Li, *Appl. Phys. Lett.*, 2013, **103**, 214101.
37 H. Morgan, N. G. G. Morgan and N. G. Green, *AC Electrokinetics: colloids and nanoparticles*, Research Studies Press, 2003, 52.
38 T. B. Jones, *Electromechanics of Particles*, 1995, 46.
39 W. Liang, S. Wang, Z. Dong, G.-B. Lee and W. J. Li, *Micromachines*, 2012, **3**, 492–508.
40 W. Liang, N. Liu, Z. Dong, L. Liu, J. D. Mai, G.-B. Lee and W. J. Li, *Sens. Actuators, A*, 2013, **193**, 103–111.

41 N. G. Green, A. Ramos and H. Morgan, *J. Phys. D: Appl. Phys.*, 2000, **33**, 632–641.
42 H. Howard Brenner, *J. Fluid Mech.*, 1962, **12**, 35–48.
43 R. Weast, M. Astle and W. Beyer, *CRC Handbook of Chemistry and Physics*, 1988, p. F-40.
44 R. Cox and H. Brenner, *Chem. Eng. Sci.*, 1967, **22**, 1753–1777.
45 M. Subbarao and G. Surya, *Int. J. Comput. Vis.*, 1994, **13**, 271–294.
46 A. Marki, E. Ermilov, A. Zakrzewicz, A. Koller, T. W. Secomb and A. R. Pries, *Biomech. Model. Mechanobiol.*, 2014, **13**, 275–288.
47 B. Lin, J. Yu and S. Rice, *Phys. Rev. E: Stat. Phys., Plasmas, Fluids, Relat. Interdiscip. Top.*, 2000, **62**, 3909–3919.
48 A. Ambari, B. Gauthier-Manuel and E. Guyon, *J. Fluid Mech.*, 1984, **149**, 235–253.
49 J. O. Marston, W. Yong and S. T. Thoroddsen, *J. Fluid Mech.*, 2010, **655**, 515–526.
50 A. Mongruel and C. Lamriben, *J. Fluid Mech.*, 2010, **661**, 229–238.
51 H. C. Berg, *Random Walks in Biology*, Princeton University Press, Princeton, 1993, p. 57.

